Struct Multidisc Optim
DOI 10.1007/s00158-009-0386-0

INDUSTRIAL APPLICATION

Inductor shape optimization for electromagnetic casting

Alfredo Canelas · Jean R. Roche · José Herskovits

Received: 29 October 2008 / Revised: 4 March 2009 / Accepted: 31 March 2009

Abstract The design of inductors in electromagnetic shaping of molten metals consists in looking for the position and the shape of a set of electric wires such that the induced electromagnetic field makes a given mass of liquid metal acquire a predefined shape. In this paper we formulate an inverse optimization problem where the position and shape of the inductors are defined by a set of design variables. In a first formulation of the inverse optimization problem we minimize the difference between the target and the equilibrium shapes while in a second approach we minimize the L^2 norm of a fictitious surface pressure that makes the target shape to be in mechanical equilibrium. Geometric constraints that prevent the inductors from penetrating the liquid metal are considered in both formulations. The optimization problems are solved using FAIPA, a line search interior-point algorithm for nonlinear optimization. Some examples are presented to show the effectiveness of the proposed approaches.

Keywords Inverse problem · Free boundary · Electromagnetic shaping · Nonlinear optimization

A. Canelas (✉)
Instituto de Estructuras y Transporte,
Facultad de Ingeniería, Universidad de la República,
J. Herrera y Reissig 565, C.P. 11300, Montevideo, Uruguay
e-mail: acanelas@fing.edu.uy

J. R. Roche
IECN, Nancy-Université, CNRS, INRIA, B.P.
70239, 54506 Vandoeuvre lès Nancy, France
e-mail: roche@iecn.u-nancy.fr

J. Herskovits
Mechanical Engineering Program - COPPE,
Federal University of Rio de Janeiro, Cidade Universitária,
Ilha do Fundão, P.O. Box 68503, CEP 21945-970, CT,
Rio de Janeiro, Brazil
e-mail: jose@optimize.ufrj.br

Present Address:
A. Canelas
Mechanical Engineering Program - COPPE,
Federal University of Rio de Janeiro, Cidade Universitária,
Ilha do Fundão, P.O. Box 68503, CEP 21945-970, CT,
Rio de Janeiro, Brazil

1 Introduction

Electromagnetic Casting (EMC) and Magnetic Suspension Melt Processing (MSMP) are important technologies in the metallurgical industry. They are based on the repulsive forces that an alternating electromagnetic field produces on the surface of diamagnetic liquid metals. They make use of the electromagnetic field for contactless heating, shaping and control of solidification of hot melts. The EMC has primarily been employed for containerless continuous casting but is mainly used to prepare ingots of aluminum alloy (Zhiqiang et al. 2002). Another important application, extensively used in aeronautics, astronautics, energy and chemical engineering, is in the manufacturing of components of engines made of superalloy materials (Ni,Ti,...) (Fu et al. 2004). Advantages of these techniques are to produce components with high surface quality, high cleanness and low contamination.

The EMC problem studied here concerns the case of a vertical column of liquid metal falling down into an electromagnetic field created by vertical inductors. In Fig. 1 the horizontal cross-section of the inductors is represented by the domains Θ_p, $1 \leq p \leq 4$, the cross-section of the liquid metal is ω, Γ is its boundary, and

Published online: 23 April 2009

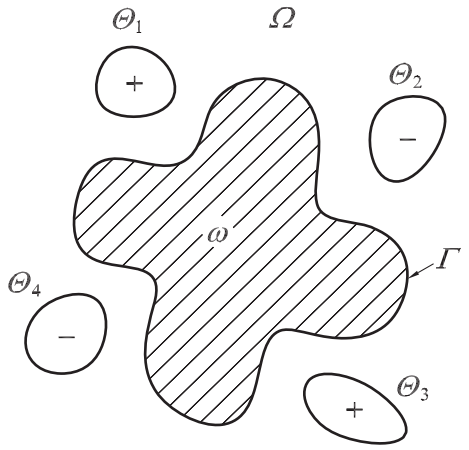

Fig. 1 EMC problem

the exterior of ω is represented in the figure by Ω. Given the position and shape of the inductors, the magnetic field created by them produces a surface pressure on the vertical column of liquid metal. That surface pressure forces the liquid metal to change its shape until an equilibrium relation on the boundary between the electromagnetic pressures and surface tensions is satisfied. The boundary shape of the liquid metal such that the equilibrium is attained can be found as the solution of a nonlinear free-surface problem, see Pierre and Roche (1991, 1993) for details. Our purpose is to design suitable inductors such that the equilibrium shape of the liquid metal be as close as possible to a given target shape.

In a previous work we studied this EMC problem considering the case where the inductors are made of single solid-core wires with a negligible area of the cross-section (Canelas et al. 2008). Thus, the inductors were represented by points in the horizontal plane. In this paper we consider the more realistic case where each inductor is a set of bundled insulated strands. In this case we represent the inductors by a set of domains in the plane as described by Fig. 1. The electric current density is assumed uniform on the entire cross-section of the inductor. This is a very reasonable approximation for the case where the inductors are made up of multiple individually insulated strands twisted or woven together.

Our goal is to determine the position and shape of the domains Θ_p in order to have a horizontal cross-section of the molten metal as close as possible to the prescribed shape. For this purpose we consider two different approaches based on the proposed in Canelas et al. (2008). The first one minimizes a distance between the computed shape and the given target one. The second approach minimizes the error of the equilibrium equation for the target shape.

In addition, here we introduce a new technique to consider geometric constraints that prevent the inductors from penetrating the liquid metal. These constraints are more suitable that the box constraints considered in Canelas et al. (2008) making the considered formulations more effective and robust for the solution of the EMC problem.

In this paper we employ a SAND formulation for both approaches and solve the optimization problems employing the *Feasible Arc Interior Point Algorithm*, FAIPA, a line search interior-point algorithm for nonlinear optimization. See (Haftka 1985; Haftka and Kamat 1989; Arora and Wang 2004, 2005; Yi et al. 2008) for a general discussion of the SAND formulation, (Achtziger 2007; Herskovits et al. 2005; Canelas et al. 2007, 2008) for some other issues and applications and (Herskovits 1998; Herskovits et al. 1996, 2005) for details about FAIPA.

The following notations are used throughout this paper:

$\mathbf{B} = (B_1, B_2, 0)$	magnetic field,
$\mathbf{J} = (0, 0, J)$	electric current density,
μ_0	magnetic permeability of the vacuum,
ω	cross-section of the liquid metal,
$\Omega = \mathbb{R}^2 \setminus \omega$	exterior of the liquid metal,
$\Gamma = \partial\omega$	liquid metal boundary,
ν	outward unit normal vector of Γ,
$\mathscr{C}$	curvature of Γ,
σ	surface tension of the liquid metal,
p_0	difference between internal and external pressures,
S_0	area of ω,
φ	magnetic flux function,
$E(\omega)$	total energy of ω,
$P(\omega)$	perimeter of ω,
m	number of inductors,
Θ_p, $1 \le p \le m$	cross-section of the inductor p,
χ_{Θ_p}	characteristic function of Θ_p,
I	reference value of the electric current density,
α_p, $1 \le p \le m$	dimensionless electric current densities,
$W^{1,\infty}(\mathbb{R}^2, \mathbb{R}^2)$	set of the Lipschitz functions from $\mathbb{R}^2$ to $\mathbb{R}^2$ such that ϕ and $\nabla\phi$ are uniformly bounded,
V, Z	maps in $W^{1,\infty}(\mathbb{R}^2, \mathbb{R}^2)$,
Id	identity map in $W^{1,\infty}(\mathbb{R}^2, \mathbb{R}^2)$,
ω_V, (Ω_V, Γ_V)	perturbed domain $(Id + V)(\omega)$,
ω^*, (Ω^*, Γ^*)	target shape,

$\omega_Z, (\Omega_Z, \Gamma_Z)$	perturbed domain $(Id + Z)(\omega^*)$,
Γ^h	piecewise approximation of Γ^*,
$\mathbf{u}$	vector of shape parameters of the liquid metal boundary,
$\Gamma_{\mathbf{u}}$	liquid metal boundary for the vector $\mathbf{u}$,
$\mathbf{u}_p$	vector of shape parameters of the inductors,
$\mathbf{q} = (q_1, \dots q_n, c)$	vector of variables of the discretized state equations,
$\mathbf{p} = (p_1, \dots p_n)$	vector of nodal fictitious pressures,
ψ	function that defines the geometric constraints.

2 The mathematical model of the electromagnetic shaping problem

We assume that the frequency of the imposed current is very high so that the magnetic field does not penetrate into the metal. Moreover, we assume that a stationary horizontal section is reached so that the two-dimensional model is valid. The equilibrium of the system is insured by the static balance on the surface of the metal between the surface tension and the electromagnetic pressure. This problem and other similar ones have been considered by several authors, we refer the reader to the following papers for the physical analysis of the simplifying assumptions that the above model requires: see (Brancher and Séro-Guillaume 1985; Gagnoud et al. 1986; Henrot and Pierre 1989; Moffatt 1985; Novruzi and Roche 1995; Pierre and Roche 1991; Shercliff 1981).

The exterior magnetic field can be found as the solution of the following boundary value problem:

$$\nabla \times \mathbf{B} = \mu_0 \mathbf{J} \quad \text{in } \Omega, \tag{1}$$

$$\nabla \cdot \mathbf{B} = 0 \quad \text{in } \Omega, \tag{2}$$

$$\mathbf{B} \cdot \nu = 0 \quad \text{on } \Gamma, \tag{3}$$

$$\|\mathbf{B}(x)\| = O(\|x\|^{-1}) \quad \text{as } \|x\| \to \infty \text{ in } \Omega. \tag{4}$$

Here the fields $\mathbf{J} = (0, 0, J)$ and $\mathbf{B} = (B_1, B_2, 0)$ represent the mean square values of the current density vector and the total magnetic field, respectively. The constant μ_0 is the vacuum permeability, ν the unit normal vector of the boundary Γ and $\|\cdot\|$ denotes the Euclidean norm. We assume that J has compact support in Ω and satisfies:

$$\int_\Omega J\, dx = 0. \tag{5}$$

On the other hand, the magnetic field produces a surface pressure that acts on the liquid metal, changing the shape until the equilibrium is attained. This equilibrium is characterized by the following equation (Pierre and Roche 1991, 1993):

$$\frac{1}{2\mu_0}\|\mathbf{B}\|^2 + \sigma \mathscr{C} = p_0 \quad \text{on } \Gamma, \tag{6}$$

where $\mathscr{C}$ is the curvature of Γ seen from the metal, σ is the surface tension of the liquid and the constant p_0 is an unknown of the problem. Physically, p_0 represents the difference between the internal and external pressures. Since it is assumed that the molten metal is incompressible, we have the following condition:

$$\int_\omega dx = S_0, \tag{7}$$

where S_0 is given.

In the direct problem the electric current density J is given and one needs to find the shape of ω that satisfies (7) and such that the magnetic field $\mathbf{B}_\omega$ solution of (1)–(4) satisfies also the equilibrium (6) for a real constant p_0.

Conditions (1)–(5), with the function J compactly supported in Ω, imply that there exists the flux function $\varphi : \Omega \to \mathbb{R}$ such that $\mathbf{B} = \left(\frac{\partial \varphi}{\partial x_2}, -\frac{\partial \varphi}{\partial x_1}, 0\right)$ and φ is the solution of:

$$\begin{aligned} -\Delta\varphi &= \mu_0 J \quad \text{in } \Omega, \\ \varphi &= 0 \quad \text{on } \Gamma, \\ \varphi(x) &= O(1) \quad \text{as } \|x\| \to \infty. \end{aligned} \tag{8}$$

The equilibrium (6) in terms of the flux φ becomes:

$$\frac{1}{2\mu_0}\|\nabla\varphi\|^2 + \sigma \mathscr{C} = p_0 \quad \text{on } \Gamma. \tag{9}$$

The direct problem, in terms of the flux, consists in looking for a domain ω such that the solution φ_ω of (8) satisfies (9) for a real constant p_0.

2.1 The variational model of the direct problem

Under suitable assumptions, the equilibrium configurations are given by the local stationary points with respect to the domain of the following total energy:

$$E(\omega) = -\frac{1}{2\mu_0}\int_\Omega \|\nabla\varphi_\omega\|^2\, dx + \sigma\, P(\omega), \tag{10}$$

subject to the equality constraint in the measure of ω:

$$\int_\omega dx = S_0. \tag{11}$$

In (10), φ_ω is the solution of (8) and $P(\omega)$ is the perimeter of ω, i.e., the length of $\Gamma = \partial\omega$ when $\partial\omega$ is regular enough (for instance of class C^1):

$$P(\omega) = \int_\Gamma d\gamma, \qquad d\gamma = \text{ length measure on } \Gamma. \tag{12}$$

The variational formulation of the direct problem consists in finding the domain ω as a stationary point of the total energy (10), subject to the constraint (11). As φ_ω is solution of (8), to prove that this variational formulation is equivalent to the previous one it remains to show that the equilibrium relation is automatically ensured for all the stationary points.

2.2 First order optimality conditions

In this section we derive the necessary condition for a domain ω to be a stationary point of the total energy (10), subject to the constraint (12). For that purpose we consider shape derivatives. Differentiation with respect to the domain is a classical issue, in this work we consider the point of view of F. Murat and J. Simon; see (Allaire 2007; Murat and Simon 1976; Simon 1980).

Let $V \in W^{1,\infty}(\mathbb{R}^2, \mathbb{R}^2)$ the set of the Lipschitz functions ϕ from $\mathbb{R}^2$ to $\mathbb{R}^2$ such that ϕ and $\nabla\phi$ are uniformly bounded (Allaire 2007). Let ω be a bounded domain in $\mathbb{R}^2$ of class C^2. We consider a shape deformation given by the mapping $Id + V$, where Id is the identity mapping. Then, the deformed domain ω_V is defined by $\omega_V = \{x + V(x) \mid x \in \omega\}$; see Fig. 2.

For every $V \in W^{1,\infty}(\mathbb{R}^2, \mathbb{R}^2)$ the mapping $Id + V$ is a diffeomorphism provided $\|V\|_{W^{1,\infty}(\mathbb{R}^2,\mathbb{R}^2)} < 1$ (Allaire 2007).

Let $\mathcal{O}(\omega)$ be the collection of images of ω considering all possible diffeomorphisms. If F is a scalar function defined in $\mathcal{O}(\omega)$ we say that it is shape differentiable if the function $V \to F(\omega_V)$ is differentiable at $V = 0$ in the Banach space $W^{1,\infty}(\mathbb{R}^2, \mathbb{R}^2)$.

The derivative of F, defined in $W^{1,\infty}(\mathbb{R}^2, \mathbb{R}^2)$, is called *shape gradient* and is denoted by $F'(\omega)$. It can be shown that the linear application $V \to F'(\omega)(V)$ is determined by the normal component of V in the boundary of ω, see the works by Allaire (2007), Novruzi and Pierre (2002) and Novruzi and Roche (1995) for a detailed description of the shape derivative structure.

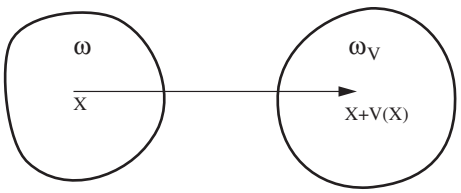

Fig. 2 Domain perturbation

Let L be the Lagrangian function defined in $\mathcal{O}(\omega) \times \mathbb{R}$ by:

$$L(\omega, p_0) = E(\omega) - p_0(m(\omega) - S_0), \tag{13}$$

Then, the first order optimality condition is the following:

$$L'(\omega, p_0)(V) = 0 \qquad \forall\, V \in W^{1,\infty}(\mathbb{R}^2, \mathbb{R}^2). \tag{14}$$

This kind of optimality conditions often appear in hydrodynamic problems and other fluid problems; let us refer for instance to the work by Shercliff (1981) where a large class of liquid metal equilibria is considered.

The next theorem shows how the term $L'(\omega, p_0)(V)$ of (14) can be calculated.

Theorem 1 *Let Ω be the complement of a compact set ω in $\mathbb{R}^2$ with nonempty interior. Assume that $\Gamma = \partial\omega = \partial\Omega$ is of class C^2. Let V be in $W^{1,\infty}(\mathbb{R}^2, \mathbb{R}^2)$ with compact support and $\|V\|_{W^{1,\infty}(\mathbb{R}^2,\mathbb{R}^2)} < 1$. Let J be a square integrable function from Ω into $\mathbb{R}$ with compact support in Ω.*

Then, there exists a unique solution φ_{ω_V} in $C^1(\overline{\Omega}_V)$ (see Kress 1999 and Henrot and Pierre 1989) of:

$$\begin{aligned} -\Delta\varphi_{\omega_v} &= \mu_0 J \quad \text{in} \quad \Omega_V, \\ \varphi_{\omega_V} &= 0 \quad \text{on} \quad \partial\Omega_V, \\ \varphi_{\omega_V}(x) &= O(1) \quad \text{as} \quad \|x\| \to \infty. \end{aligned} \tag{15}$$

and the shape derivative of the lagrangian L is given by:

$$L'(\omega, p_0)(V) = \int_\Gamma \left(\frac{1}{2\mu_0} \|\nabla\varphi_\omega\|^2 + \sigma\mathscr{C} - p_0 \right)(V \cdot \nu)\, d\gamma, \tag{16}$$

where ν is the unit normal vector of Γ oriented toward Ω, $\mathscr{C}$ is the curvature of Γ (seen from the metal) and φ_ω the solution of (8).

Proof See (Henrot and Pierre 1989; Pierre and Roche 1991; Novruzi and Roche 1995; Allaire 2007). □

This problem is very similar to some ones considered by several authors. We refer the readers to the following papers and references therein for the physical analysis of the simplifying assumptions that the above model requires: see (Brancher and Séro-Guillaume 1985; Coulaud and Henrot 1994; Gagnoud et al. 1986; Henrot and Pierre 1989; Henrot et al. 1989; Moffatt 1985; Novruzi 1997; Novruzi and Roche 1995, 2000; Pierre and Roche 1991, 1993; Roche 1996, 1997;

Séro-Guillaume et al. 1992; Sneyd and Moffatt 1982; Zouaoui et al. 1990).

3 The inverse problem

From a practical point of view, the magnetic field has to be created by a simple configuration of inductors. For that purpose, we consider a distribution of the electric current density J of the form:

$$J = I \sum_{p=1}^{m} \alpha_p \chi_{\Theta_p}, \tag{17}$$

where I is a given intensity of current, Θ_p, with $1 \leq p \leq m$, are subsets of $\mathbb{R}^2$, χ_{Θ_p} are their characteristic functions, and α_p are dimensionless coefficients. The inverse problem consists in determining the sets Θ_p.

Note that the expression (17) assumes that the electric current density is uniform on each region Θ_p. Inductors made of bundled insulated strands allow the use of (17) as a good approximation, see (Sullivan 1999) and references therein. They are also suitable to make inductors of specific geometries.

For an electric current density given by (17), (5) is satisfied imposing:

$$\sum_{p=1}^{m} \alpha_p \int_{\Theta_p} dx = 0. \tag{18}$$

Given the target shape ω^*, we want to find the domains Θ_p, $1 \leq p \leq m$, as the solution of the following optimization problem:

$$\min_{\Theta_1,\ldots,\Theta_m} \mathrm{d}(\omega, \omega^*), \tag{19}$$

where the function d is a distance between ω and ω^*. The domain ω belongs to the set of admissible domains, i.e., $\omega \in \mathscr{O}$, and is in equilibrium under the action of the electric current density J of (17) in the variational sense. In other words, ω satisfies the area constraint (11) and the flux φ_ω solution of (8) satisfies the equilibrium equation (20) for a real constant p_0:

$$\int_\Gamma \left(\frac{1}{2\mu_0} \|\nabla \varphi_\omega\|^2 + \sigma \mathscr{C} - p_0 \right) (V \cdot \nu)\, d\gamma = 0$$
$$\forall\, V \text{ in } C^1(\mathbb{R}^2, \mathbb{R}^2). \tag{20}$$

In certain cases it is possible to find a current density distribution such that the target shape ω^* is in equilibrium. This topic was already studied and there are a few papers about the existence of such solutions. See (Henrot and Pierre 1989; Felici and Brancher 1991; Pierre and Rouy 1996). However, a solution given by the addition of a finite number of characteristic functions like (17) may be not possible. See (Henrot and Pierre 1989) and (Canelas et al. 2008).

3.1 Two approaches for the inverse problem

We propose two different approaches for finding an approximate solution of problem (19). The first one considers a domain deformation of ω^* defined by the mapping:

$$T_Z(x) = x + Z(x), \quad \forall\, x \in \mathbb{R}^2, \tag{21}$$

where Z is a regular vector field with compact support in $\mathbb{R}^2$. Then, defining:

$$\omega_Z = T_Z(\omega^*),$$
$$\Gamma_Z = T_Z(\Gamma^*).$$

The formulation of the first inverse problem, with J defined by (17) is:

$$\min_{\Theta_1,\ldots,\Theta_m, Z} \| Z \|^2_{L^2(\Gamma^*)},$$

subject to:

$$\omega_Z \text{ is in equilibrium under } J. \tag{22}$$

Note that in this formulation Z is considered independent of the domains Θ_p. We can think about Problem (22) as a formulation that start from the target domain ω^*, and looks for the smaller deformation such that the deformed domain ω_Z can be in equilibrium for the electric current defined by the domains Θ_p.

A second formulation of the inverse problem can be considered introducing a slack variable function $p(x) : \Gamma \to \mathbb{R}$ in order to make the equilibrium equation satisfied for the target shape:

$$\int_{\Gamma^*} \left(\frac{1}{2\mu_0} \|\nabla \varphi_\omega\|^2 + \sigma \mathscr{C} - p_0 + p \right) (V \cdot \nu)\, d\gamma = 0$$
$$\forall\, V \text{ in } C^1(\mathbb{R}^2, \mathbb{R}^2). \tag{23}$$

The function p can be understood as an additional pressure acting on the interface. Given J and ω^*, p is the surface pressure that equilibrates the action of the magnetic pressure and the surface tension. The second formulation for the inverse problem is an indirect approach that try to minimize the $L^2(\Gamma^*)$ norm of the function p:

$$\min_{\Theta_1,\ldots,\Theta_m, p} \| p \|^2_{L^2(\Gamma^*)},$$

subject to:

$$\omega^* \text{ is in equilibrium under } J \text{ and } p. \tag{24}$$

In this last formulation only shape variables concerning the inductors are considered. This fact makes (24) much easier to solve than (22). If the function p vanishes at the solution of (24), the optimal domains Θ_p will also be a solution of the first formulation with the equilibrium domain matching exactly the target shape. In the general case, p will not vanish at the solution and, in this case, the target shape ω^* will not be in equilibrium under J only. Then, a second stage of analysis will be necessary to find the equilibrium domain under the obtained current density distribution. However, as the norm of p was minimized, the resultant equilibrium domain is expected to be a good approximation of the target one. Furthermore, since (24) can be solved with a minor computational effort, its solution J can be employed as an initial guess for the formulation (22).

4 Numerical method

4.1 The exterior Dirichlet problem

To solve (8) in the exterior domain Ω we consider a particular solution φ_1 of the differential equation given by:

$$\varphi_1(x) = -\frac{\mu_0}{2\pi}\int_{\mathbb{R}^2} \ln\|x-y\| J(y)\, dy. \tag{25}$$

This function is a solution of the problem:

$$-\Delta\varphi_1(x) = \mu_0 J \qquad \text{in } \mathbb{R}^2, \tag{26}$$

$$\varphi_1(x) = O(1) \quad \text{as } \|x\| \to \infty. \tag{27}$$

Note that for the current density distribution defined by (17), the expression of φ_1 is

$$\varphi_1(x) = -\frac{\mu_0 I}{2\pi}\sum_{p=1}^{m}\alpha_p \int_{\Theta_p} \ln\|x-y\|\, dy. \tag{28}$$

The function φ_1 can be calculated as a sum of line integrals on the boundaries Γ_p of domains Θ_p. Consider the function $w : \mathbb{R}^2 \times \mathbb{R}^2 \to \mathbb{R}^2$ defined as:

$$w(x,y) = (1/4)(1 - 2\ln\|x-y\|)(x-y). \tag{29}$$

The divergence of w is $\nabla_y \cdot w = \ln\|x-y\|$. Then, (28) becomes:

$$\varphi_1(x) = -\frac{\mu_0 I}{2\pi}\sum_{p=1}^{m}\alpha_p \int_{\Gamma_p} w(x,y)\cdot \nu\, d\gamma. \tag{30}$$

The function φ can be computed as:

$$\varphi(x) = \xi(x) + \varphi_1(x), \tag{31}$$

where the function ξ is the solution of the following exterior problem:

$$\begin{aligned} -\Delta\xi(x) &= 0 && \text{in } \Omega,\\ \xi(x) &= -\varphi_1(x) && \text{on } \Gamma,\\ \|\xi(x)\| &= O(1) && \text{as } \|x\| \to \infty. \end{aligned} \tag{32}$$

Following Kress (1999), an integral single layer representation of the solution of (32) is given by:

$$\xi(x) = -\frac{1}{2\pi}\int_\Gamma q(y)\ln\|x-y\|\, d\gamma + c, \tag{33}$$

where the constant c is the value at the infinity of ξ and the function $q(y) \in H^{-1/2}(\Gamma)$ satisfies:

$$\int_\Gamma q(y)\, d\gamma = 0. \tag{34}$$

It remains to impose the boundary conditions on Γ. Here, this is done with a weak formulation. Let $a_\Gamma(q,g)$ be the following elliptic bilinear form:

$$\begin{aligned} a_\Gamma(q,g) = &-\frac{1}{2\pi}\int_\Gamma g(x)\int_\Gamma q(y)\ln\|x-y\|\, d\gamma\, d\gamma\\ &+ c\int_\Gamma g(x)\, d\gamma \end{aligned} \tag{35}$$

defined on $H^{-1/2}(\Gamma)\times H^{-1/2}(\Gamma)$. We look for a function $q(y) \in H^{-1/2}(\Gamma)$ that satisfies (34) and:

$$a_\Gamma(q,g) = -\int_\Gamma \varphi_1(x) g(x)\, d\gamma \quad \forall\, g \in H^{-1/2}(\Gamma). \tag{36}$$

Equation (36) with φ_1 given by (30) will be used instead of (8). Note that the unknown variables are now the function q and the scalar c.

Finally, the norm $\|\nabla\varphi\|$ in the equilibrium (20) can be computed as:

$$\|\nabla\varphi\| = \left|\frac{\partial\varphi}{\partial\nu}\right| = \left|\frac{\partial\varphi_1}{\partial\nu} + \frac{\partial\xi}{\partial\nu}\right|, \tag{37}$$

where the first equality comes from the fact that φ is constant on Γ, and the second one from (31). The normal derivative of φ_1 is obtained from (30):

$$\frac{\partial\varphi_1}{\partial\nu_x}(x) = -\frac{\mu_0 I}{2\pi}\sum_{p=1}^{m}\alpha_p \int_{\Gamma_p}\frac{\partial}{\partial\nu_x}(w(x,y)\cdot\nu)\, d\gamma. \tag{38}$$

The following expression can be used for ξ:

$$\begin{aligned} \frac{\partial\xi}{\partial\nu_x}(x) = &-\frac{1}{2\pi}\int_\Gamma q(y)\frac{\partial}{\partial\nu_x}\ln\|x-y\|\, d\gamma\\ &+\frac{1}{2}q(x) \quad \forall\, x \in \Gamma, \end{aligned} \tag{39}$$

where the integral of (39) is understood in the Cauchy principal value sense.

4.2 The SAND formulation of the inverse problems

A SAND formulation of the inverse problems (22) and (24) is employed here. In other words, the state variables p_0, c and q are incorporated as unknowns of the optimization problem and the state and equilibrium equations are incorporated as equality constraints. The optimization problem of the formulation (22) becomes:

$$\min_{J,Z,p_0,c,q} \|Z\|^2_{L^2(\Gamma^*)}, \tag{40}$$

subject to the area constraint:

$$\int_{\omega_Z} dx = S_0, \tag{41}$$

the state equations:

$$a_{\Gamma_Z}(q,g) = -\int_{\Gamma_Z} \varphi_1(x) g(x)\, d\gamma \quad \forall\, g \in H^{-1/2}(\Gamma_Z), \tag{42}$$

$$\int_{\Gamma_Z} q(y)\, d\gamma = 0, \tag{43}$$

and the equilibrium equation:

$$\int_{\Gamma_Z} \left(\frac{1}{2\mu_0} \|\nabla\varphi\|^2 + \sigma\mathscr{C} - p_0 \right) (V\cdot\nu)\, d\gamma = 0 \quad \forall\, V \text{ in } C^1(\mathbb{R}^2,\mathbb{R}^2), \tag{44}$$

where φ_1, φ, and ξ are given by (25), (31) and (33).

The optimization problem of the formulation (24) becomes:

$$\min_{J,p,p_0,c,q} \|p\|^2_{L^2(\Gamma^*)}, \tag{45}$$

subject to the state equations:

$$a_{\Gamma^*}(q,g) = -\int_{\Gamma^*} \varphi_1(x) g(x)\, d\gamma \quad \forall\, g \in H^{-1/2}(\Gamma^*), \tag{46}$$

$$\int_{\Gamma^*} q(y)\, d\gamma = 0, \tag{47}$$

and the equilibrium equation:

$$\int_{\Gamma^*} \left(\frac{1}{2\mu_0} \|\nabla\varphi\|^2 + \sigma\mathscr{C} - p_0 + p \right) (V\cdot\nu)\, d\gamma = 0 \quad \forall\, V \text{ in } C^1(\mathbb{R}^2,\mathbb{R}^2). \tag{48}$$

4.3 The numerical model

4.3.1 Discretization of the domain

We consider an approximation of the domain ω^* defined by the piecewise linear closed boundary Γ^h, i.e., Γ^h is the union of the n linear finite elements ℓ_j in $\mathbb{R}^2$, $j \in \{1,\ldots,n\}$. The nodes of the boundary Γ^h are denoted by x_i.

A direction $\hat{Z}^i \in \mathbb{R}^2$ is associated to each vertex x_i of Γ^h. We construct a continuous piecewise linear vector field Z^i from Γ^h in $\mathbb{R}^2$ such that $Z^i(x_k) = \delta_{ik}\hat{Z}^i$. The support of Z^i is equal to the union of the finite elements for which x_i is a node. The vector field Z of (21) is computed as:

$$Z(x) = \sum_{i=1}^{n} u_i Z^i(x), \tag{49}$$

and the updated boundary $\Gamma_{\mathbf{u}}$ is then given by:

$$\Gamma_{\mathbf{u}} = \left\{ X \mid X = x + Z(x);\ u_i \in \mathbb{R},\ x \in \Gamma^h \right\}, \tag{50}$$

where $\mathbf{u}^T = (u_1,\ldots,u_n) \in \mathbb{R}^n$ is the vector of unknowns which determine the evolution of the boundary. This representation has the advantage of defining only one degree of freedom for each node. We denote by $\omega_{\mathbf{u}}$ the interior domain related to $\Gamma_{\mathbf{u}}$ in order to show the dependence with respect to the vector $\mathbf{u}$.

4.3.2 Inductors

We consider inductors with a transversal cross-section corresponding to one of the parametric shapes given by Fig. 3. The contribution of each inductor to the function φ_1 is calculated using (30). The boundary Γ_p of each inductor is divided in small linear elements to perform

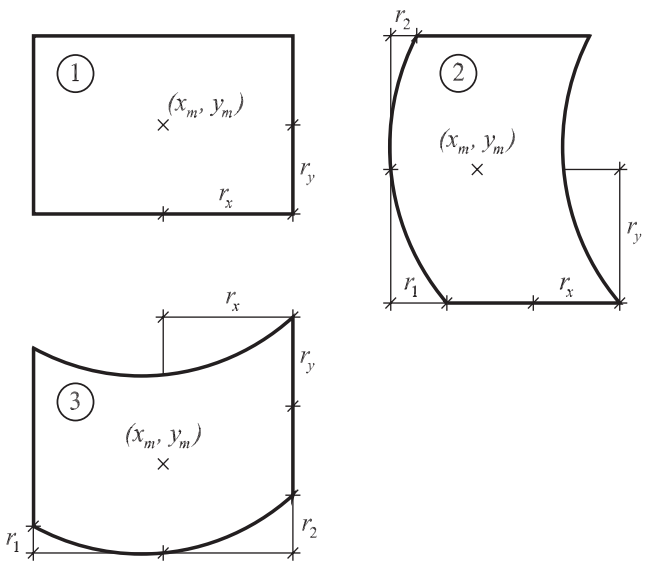

Fig. 3 Parametric shape of the cross-section of the inductors. *1.* four-parameter inductor of rectangular cross-section; *2.* six-parameter inductor of parabolic vertical sides; *3.* six-parameter inductor of parabolic horizontal sides

the integration. The entire set of shape parameters corresponding to the inductors is denoted by $\mathbf{u}_p$.

4.3.3 Exterior boundary value problem

For numerical calculations we consider a piecewise constant approximation $q_h(x)$ of $q(x)$:

$$q_h(x) = \sum_{j=1}^{n} q_j e_j(x), \tag{51}$$

where $e_j(x) = 1$ if $x \in \ell_j$ and zero elsewhere.

Replacing the function g in (42) by e_i, with $i \in \{1, \ldots, n\}$, the weak formulation of the boundary value problem, given by (42) and (43), becomes:

$$\mathbf{A}(\mathbf{u})\mathbf{q} = \mathbf{b}(\mathbf{u}_p, \mathbf{u}), \tag{52}$$

where the vector $\mathbf{q}^T = (q_1, \ldots, q_n, c)$ is in $\mathbb{R}^{n+1}$, $\mathbf{u}$ is the vector of shape variables and $\mathbf{u}_p$ is the vector that contains the shape parameters of the inductors. The coefficients a_{ij} of the symmetric matrix $\mathbf{A}(\mathbf{u})$ are:

$$a_{ij}(\mathbf{u}) = -\frac{1}{2\pi} \int_{\ell_i}\int_{\ell_j} \ln \|x - y\| \, d\gamma \, d\gamma \quad i, j \in \{1, \ldots, n\}, \tag{53}$$

$$a_{ij}(\mathbf{u}) = \int_{\ell_j} d\gamma \qquad i = n+1, \text{ and } j \in \{1, \ldots, n\}, \tag{54}$$

and the components b_i of the vector $\mathbf{b}$ are:

$$b_i(\mathbf{u}_p, \mathbf{u}) = -\int_{\ell_i} \varphi_1(x) \, d\gamma \qquad i \in \{1, \ldots, n\}, \tag{55}$$

$$b_i(\mathbf{u}_p, \mathbf{u}) = 0 \qquad i = n+1, \tag{56}$$

For given vectors $\mathbf{u}$ and $\mathbf{u}_p$, the linear system (52) is symmetric and non-sparse. Numerical approximations of the element integrals of previous and later equations are computed by Gauss quadrature.

If q is the solution of the system (34), (36) and the piecewise constant approximation q_h given by the solution of (52), then we have the following error bounds (see Nédélec 1977):

$$\|q - q_h\|_{H^{-1/2}(\Gamma)} \leq C_1 h \|q\|_{H^1(\Gamma)}, \tag{57}$$

and if ξ_h is the approximation of (33) then

$$\left\| \frac{\partial \xi}{\partial \nu} - \frac{\partial \xi_h}{\partial \nu} \right\|_{H^{-1/2}(\Gamma)} \leq C_2 h \|q\|_{H^1(\Gamma)}. \tag{58}$$

The approximation of the normal derivative $\frac{\partial \xi}{\partial \nu}$ at $x_l \in \ell_l$ is given by:

$$\frac{\partial \xi_h}{\partial \nu}(x_l) = -\frac{1}{2\pi} \sum_{\substack{i=1 \\ i \neq l}}^{n} q_i \sum_{m=1}^{K} p_m \frac{\partial \ln \|x_l - x_i(s_m)\|}{\partial \nu} + \frac{1}{2} q_l, \tag{59}$$

where $x_i(s_m)$ are the integration points and p_m the weights of the Gauss quadrature formula. Thus, the computation of $\frac{\partial \xi_h}{\partial \nu}(x_l)$ needs $O(n)$ floating point operations.

4.3.4 Equilibrium equation

Consider a direction $\hat{V}^i \in \mathbb{R}^2$ associated to each vertex x_i of Γ^h and the continuous piecewise linear vector field V^i from Γ^h in $\mathbb{R}^2$ such that $V^i(x_k) = \delta_{ik}\hat{V}^i$. If we project (44) in the finite dimensional space generated by $V^i, i \in \{1, \ldots, n\}$, the discrete version of the equilibrium is the following:

$$DE_i(\mathbf{u}_p, \mathbf{u}, \mathbf{q}, p_0) = \int_{\Gamma_\mathbf{u}} \left(\frac{1}{2\mu_0} \|\nabla \varphi\|^2 - p_0 \right) (V^i \cdot \nu) \, d\gamma + \sigma \mathscr{C}^i \cdot \hat{V}^i, \tag{60}$$

where $i \in \{1, \ldots, n\}$ and $\mathscr{C}^i$ is an approximation of the mean curvature at x_i, given by:

$$\mathscr{C}^i = \left(\frac{(x_i - x_{i-1})}{\|x_i - x_{i-1}\|} - \frac{(x_{i+1} - x_i)}{\|x_{i+1} - x_i\|} \right). \tag{61}$$

The gradient $\nabla \varphi$ is computed using (37)–(39).

In the case of (48), we consider a piecewise linear function p_h defined as:

$$p_h(x) = \sum_{i=1}^{n} p_i f_i, \tag{62}$$

where the function f_i satisfies $f_i(x_k) = \delta_{ik}$. Then, defining $\mathbf{p}^T = (p_1, \ldots, p_n)$, the equilibrium equation is defined as:

$$DF_i(\mathbf{u}_p, \mathbf{p}, \mathbf{q}, p_0) = \frac{1}{2\mu_0} \int_{\Gamma^*} (\|\nabla \varphi\|^2 - p_0 + p_h)(V^i \cdot \nu) \, d\gamma + \sigma \mathscr{C}^i \cdot \hat{V}^i. \tag{63}$$

4.4 Geometric constraints

In order to avoid the possibility of overlapping between the domains occupied by the liquid metal and the inductors, we propose a new approach that consists in considering the following inequalities:

$$\psi(x_j) \leq \psi_0, \quad \text{for all } x_j \in \mathbf{X}, \tag{64}$$

where $\mathbf{X}$ is a chosen set of points belonging to the boundary of the inductors. The real valued function ψ is zero in the interior of the liquid metal and negative in the exterior. Then, choosing a negative value for the parameter ψ_0, (64) enforces the points x_j to be in the exterior of the liquid metal as illustrated by Fig. 4.

The function ψ that we propose is defined as the solution of:

$$\begin{aligned} \Delta\psi(x) &= 0 \quad \text{in } \Omega^*, \\ \psi(x) &= 0 \quad \text{on } \Gamma^*, \\ \int_{\Gamma^*} \nabla\psi(x)\cdot\nu\, d\gamma &= -1. \end{aligned} \tag{65}$$

In a similar way as the function ξ in Section 4.1, ψ can be calculated as:

$$\psi(x) = -\frac{1}{2\pi}\int_{\Gamma} q(y)\ln\|x-y\|\, d\gamma + c, \tag{66}$$

where q must satisfy:

$$\int_{\Gamma} q(y)\, d\gamma = -1. \tag{67}$$

As in Section 4.3.3, an approximated solution of q and c can be obtained solving a linear system similar to (52). The numerical approximation of the function ψ is obtained employing (66).

The value ψ_0 can be defined choosing a point in the exterior of the liquid metal and calculating the value of the function ψ at this point. See Figs. 5 and 6 that show the function ψ for two different target shapes.

Defining $\mathbf{h}_j(\mathbf{u}_p) = \psi(x_j(\mathbf{u}_p)) - \psi_0$, all the geometric constraints are expressed as:

$$\mathbf{h}(\mathbf{u}_p) \le 0. \tag{68}$$

Note that the function ψ was defined for the fixed domain Ω^*. Then, strictly speaking, the constraints (64) are suitable just for the the second formulation of the inverse problem. In the case of the first formulation, ψ should be defined for the changing domain Ω_Z. In that case there is an extra computational cost associated to the computation of q and c each time that the domain Ω_Z is updated. However, we have observed for all the examples considered that the use of ψ defined for the fixed domain Ω^* is enough to prevent the overlapping between domains. The reason is that the domain occupied by the liquid metal keeps very close to the target shape all along the optimization process. Only the inductors experiment big shape changes but the constraints (64) are effective to keep them away from the target shape.

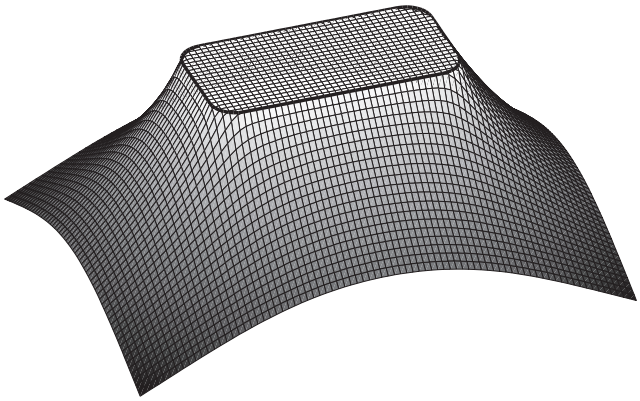

Fig. 5 Function ψ for a rectangular like target shape

4.5 Discretized inverse problems

Consider the area function $S(\mathbf{u}) = \int_{\omega_\mathbf{u}} dx$, and the vector function $DE(\mathbf{u}_p, \mathbf{u}, \mathbf{q}, p_0)$, such that $(DE)_i =$

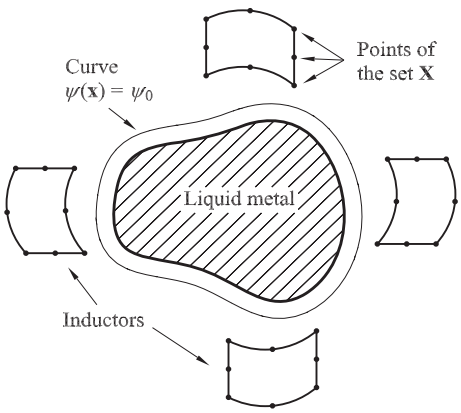

Fig. 4 Geometric constraints

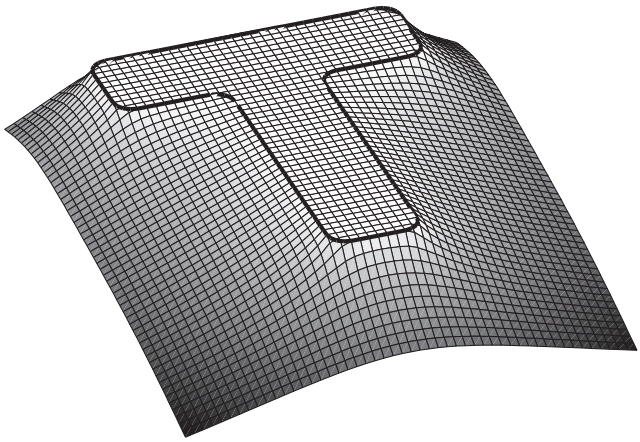

Fig. 6 Function ψ for a "T" like target shape

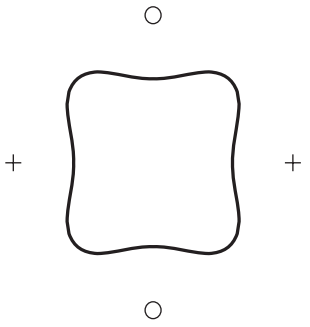

Fig. 7 Example 1, target shape considering concentrated intensities. *Solid line*: equilibrium shape, *plus*: positive current, *circle*: negative current

$DE_i(\mathbf{u}_p, \mathbf{u}, \mathbf{q}, p_0)$. The discretized version of the first inverse problem is the following:

$$\min_{\mathbf{u}_p, \mathbf{u}, \mathbf{q}, p_0} \| Z \|^2_{L^2(\Gamma^*)}, \tag{69}$$

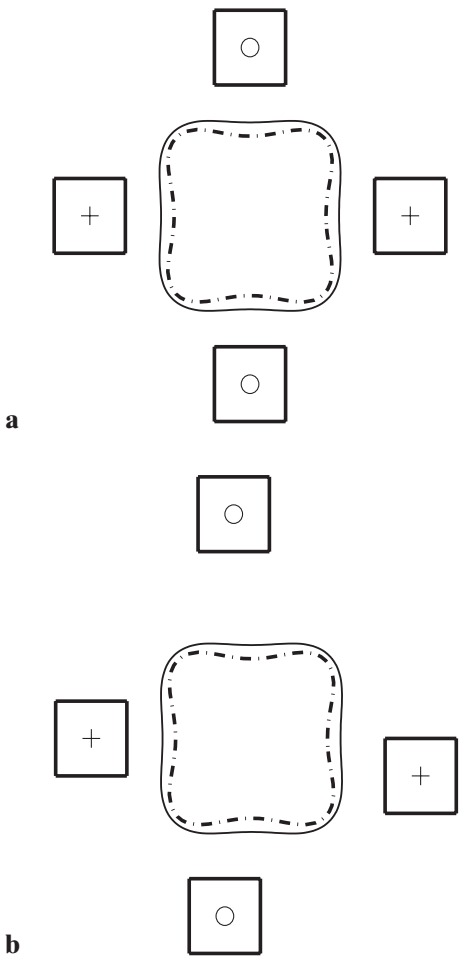

Fig. 8 Example 1, initial configuration and geometric constraints of examples Ex1a and Ex1b, **a** example Ex1a. **b** example Ex1b. *Dash-dot line*: target shape, *solid line*: curve $\psi(x) = \psi_0$, *plus*: inductor of positive current, *circle*: inductor of negative current

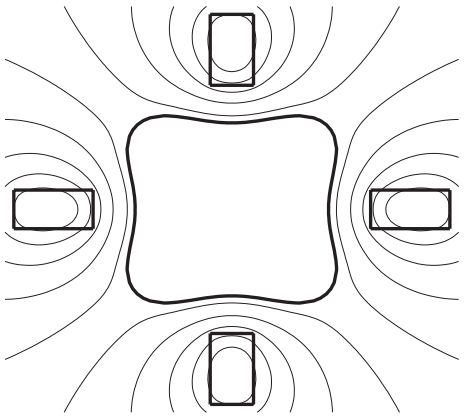

Fig. 9 Solution of the Example 1, both formulations, equilibrium shape and level curves of the flux function φ

subject to the nonlinear equality constraints:

$$\begin{pmatrix} \mathbf{A}(\mathbf{u})\mathbf{q} - \mathbf{b}(\mathbf{u}_p, \mathbf{u}) \\ S(\mathbf{u}) - S_0 \\ DE(\mathbf{u}_p, \mathbf{u}, \mathbf{q}, p_0) \end{pmatrix} = 0, \tag{70}$$

and the nonlinear inequalities:

$$\mathbf{h}(\mathbf{u}_p) \leq 0. \tag{71}$$

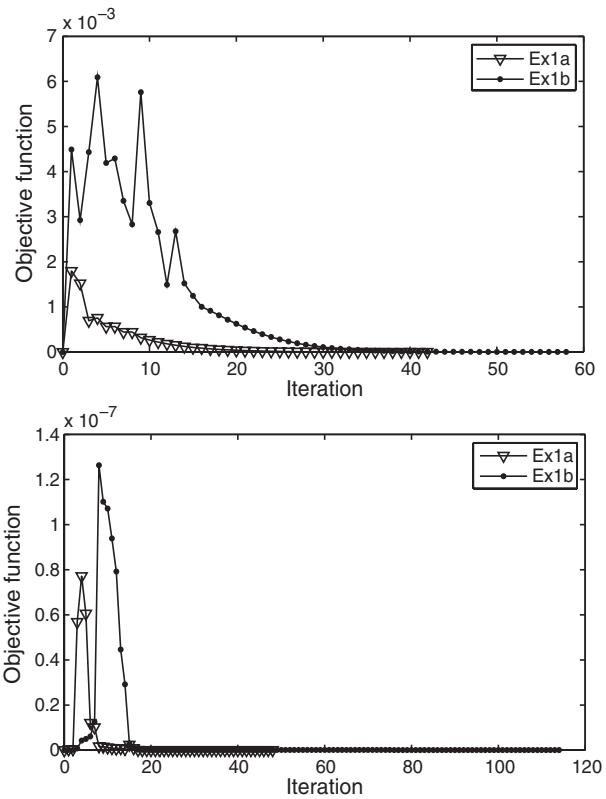

Fig. 10 Example 1, evolution of the objective functions, **a** first formulation, **b** second formulation

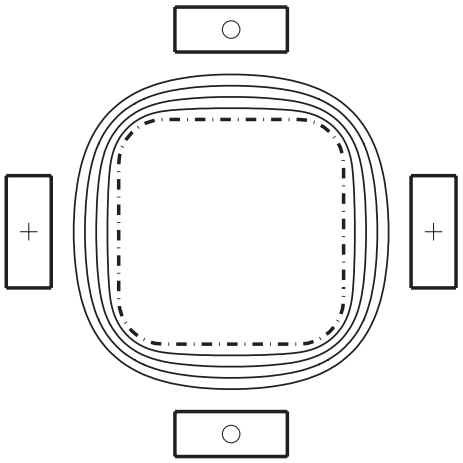

Fig. 11 Example 2, initial configuration and geometric constraints of examples Ex2a to Ex2d. *Dash-dot line*: target shape, *solid line*: curves $\psi(x) = \psi_0$ for four different values of ψ_0, *plus*: inductor of positive current, *circle*: inductor of negative current

The discretized version of the second inverse problem is:

$$\min_{\mathbf{u}_p, \mathbf{q}, c, p_0} \|p\|^2_{L^2(\Gamma^*)}, \tag{72}$$

with the equality constraints:

$$\begin{pmatrix} \mathbf{A}\mathbf{q} - \mathbf{b}(\mathbf{u}_p) \\ DF(\mathbf{u}_p, \mathbf{p}, \mathbf{q}, p_0) \end{pmatrix} = 0, \tag{73}$$

and the nonlinear inequalities:

$$\mathbf{h}(\mathbf{u}_p) \leq 0. \tag{74}$$

In this case, since the integrals are defined on the fixed domain Γ^* the vector $\mathbf{u}$ of shape variables is not present in the formulation.

5 Numerical examples

We consider several examples to illustrate the behavior of the proposed formulations of the inverse problem. The goal is to identify the position and shape of the inductors given by the shape variables $\mathbf{u}_p$. The shape and the surface S_0 of the target shape, the surface tension σ, the intensity I and the dimensionless coefficients α_p are given. For each example all the parameters, including the parameters ψ_0 of the geometric constraints, are the same for both formulations. The initial values of the state variables $\mathbf{q}$ and p_0, the shape variable $\mathbf{u}$ of the first

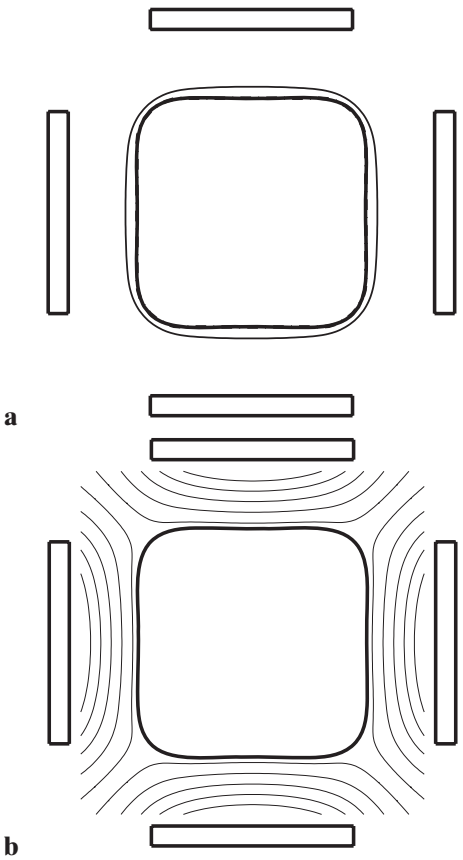

Fig. 12 Solution of example Ex2a, first formulation, **a** solution and geometric constraint, **b** equilibrium shape and level curves of the flux function φ

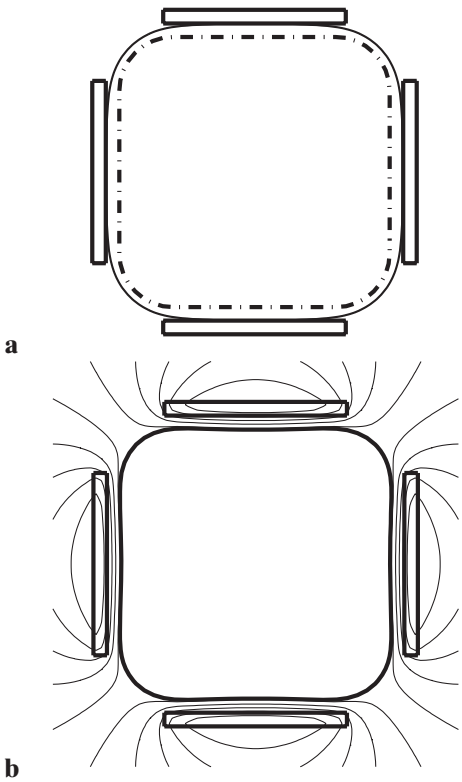

Fig. 13 Solution of example Ex2a, second formulation, **a** solution and geometric constraint, **b** equilibrium shape and level curves of the flux function φ

formulation and the pressure **p** of the second one are set equal to zero for all the examples.

For the solution of the optimization problems, the line search interior-point algorithm for nonlinear constrained optimization problems FAIPA was employed. For a given feasible point with respect to the inequality constraints, FAIPA defines a feasible and descent arc solving three linear systems of equations with the same coefficient matrix. Then, it performs a line search along this arc to define the next point. FAIPA makes subsequent iterations until a convergence criterion is satisfied. In this paper we accept the actual point if the norm of the equality constraints is less than 1.0×10^{-6} and the reduction of the objective function with respect to the value at the previous iteration is less than 0.1%.

At each iteration FAIPA needs the vector of partial derivatives with respect to all the design variables of the objective function and all the constraints. Herein, we have calculated exact derivatives for all the functions of the discretized model; see (Choi and Kim 2004). For more details about FAIPA see (Herskovits 1998; Herskovits et al. 1996, 2005).

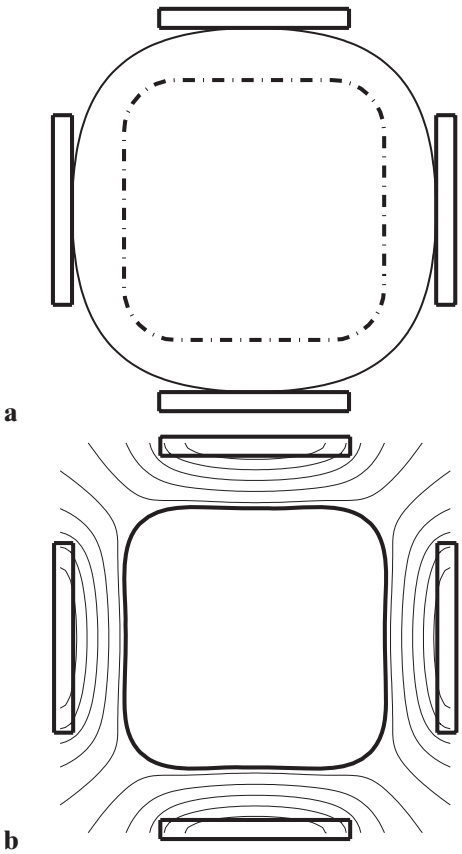

Fig. 14 Solution of example Ex2d, second formulation, **a** solution and geometric constraint, **b** equilibrium shape and level curves of the flux function φ

For each example we plot the initial position and shape of the inductors, the target shape of the liquid metal, the shape of the inductors obtained by the optimization algorithm and the evolution of the objective function during the iterative process.

5.1 Example 1

The target shape of this example is the solution of the direct free-surface problem considering four concentrated intensities of value $I = 0.1$, with the sign given by Fig. 7; see (Canelas et al. 2008, Example 1a).

For the inverse problem we consider four inductors of type 1 of Fig. 3, and a target shape of area S_0 equal to π. The intensity I is equal to 0.1 and the surface tension σ is equal to 1.0×10^{-4}. The dimensionless coefficients α_p have absolute value equal to 4.0 with the sign given by Fig. 8; two configurations for the initial positions of the inductors, named Ex1a and Ex1b, are considered as depicted by the figure.

The configuration of inductors obtained was the same for both initial configurations and both formulations. The equilibrium shape obtained is almost the same as the target one and none of the geometric

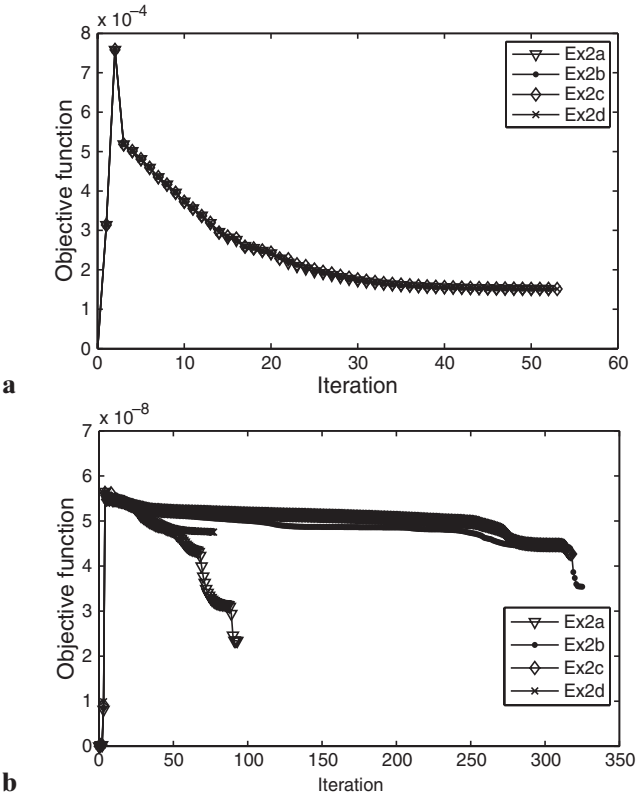

Fig. 15 Example 2, evolution of the objective functions, **a** first formulation, **b** second formulation

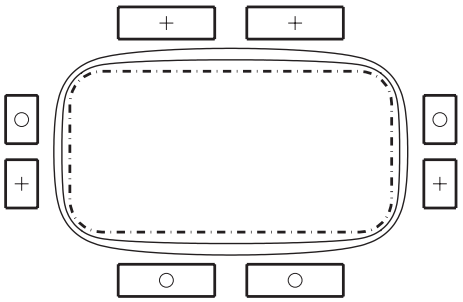

Fig. 16 Example 3, initial configuration and geometric constraints of examples Ex3a and Ex3b. *Dash-dot line*: target shape, *solid line*: curves $\psi(x) = \psi_0$ for four different values of ψ_0, *plus*: inductor of positive current, *circle*: inductor of negative current

constraints is active at the solution. Figure 9 shows the inductors obtained and some level curves of the flux function φ at the solution. Figure 10 shows the evolution of the objective function during the iterative process.

Note that the objective functions of both formulations vanish in the beginning due to the choice of the initial values of vectors **u** and **p**. Then, as the equality constraints are not satisfied, the value of the objective function increases in the initial iterations. After some iterations the value of the objective function reaches a maximum and decreases in subsequent iterations. At the end of the iterative process the objective function reaches the optimum value and the equality constraints are satisfied.

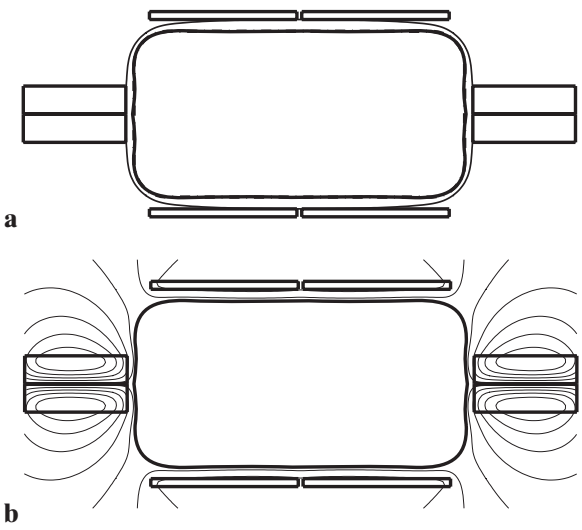

Fig. 17 Solution of example Ex3a, first formulation, **a** solution and geometric constraint, **b** equilibrium shape and level curves of the flux function φ

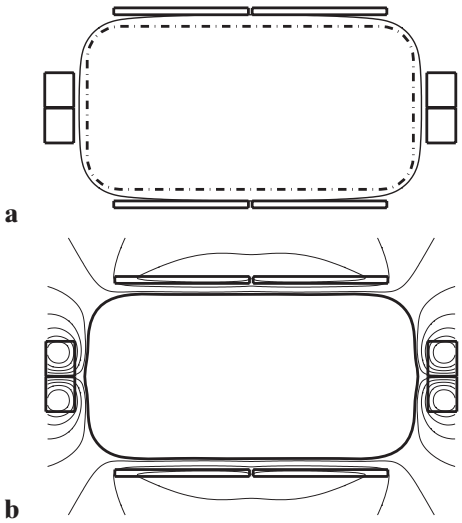

Fig. 18 Solution of example Ex3a, second formulation, **a** solution and geometric constraint, **b** equilibrium shape and level curves of the flux function φ

5.2 Example 2

In this example the target shape is the rounded square depicted by Fig. 11. For the inverse problem we consider four inductors of type 1 of Fig. 3, and a target shape of area S_0 equal to 3.86. The intensity I is equal

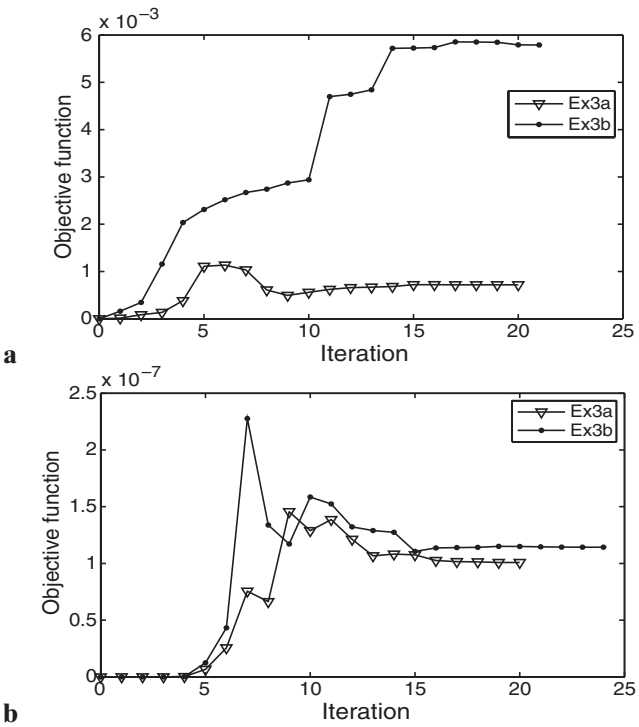

Fig. 19 Example 3, evolution of the objective functions, **a** first formulation, **b** second formulation

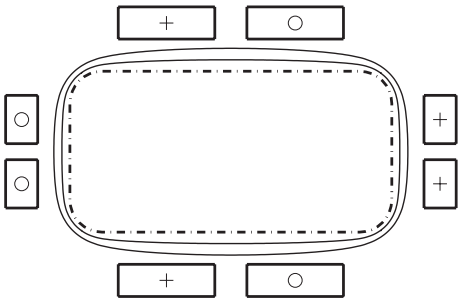

Fig. 20 Example 4, initial configuration and geometric constraints of examples Ex4a and Ex4b. *Dash-dot line*: target shape, *solid line*: curves $\psi(x) = \psi_0$ for four different values of ψ_0, *plus*: inductor of positive current, *circle*: inductor of negative current

to 0.1 and the surface tension σ is equal to 1.0×10^{-4}. The dimensionless coefficients α_p have absolute value equal to 4.0 with the sign given by Fig. 11. Four different values of the parameter ψ_0 of the geometric constraints are considered, these values generate four different problems that we have named Ex2a to Ex2d, as shown by the Fig. 11. The example Ex2a corresponds to the constraint given by the closest curve to the target shape while the example Ex2d corresponds to the the farthest one.

For the first formulation, the same configuration of inductors was obtained for all cases as shown by Fig. 12a; the equilibrium shape and some level curves

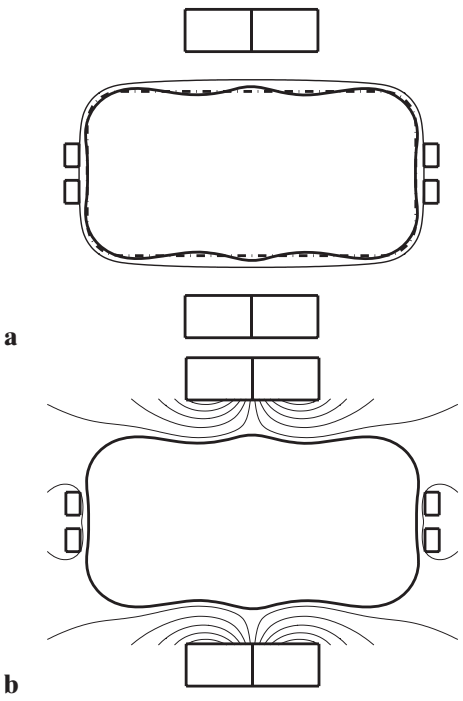

Fig. 21 Solution of example Ex4a, first formulation, **a** solution and geometric constraint, **b** equilibrium shape and level curves of the flux function φ

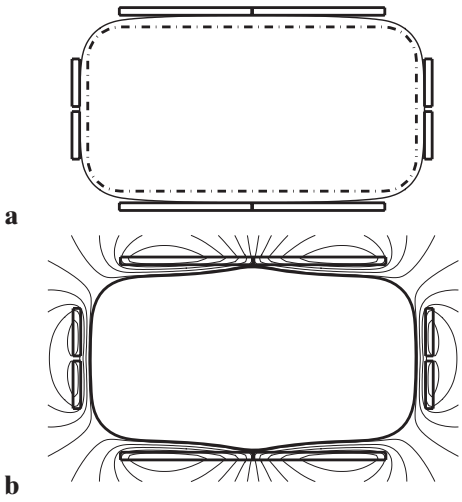

Fig. 22 Solution of example Ex4a, second formulation, **a** solution and geometric constraint, **b** equilibrium shape and level curves of the flux function φ

of the flux function φ at the solution is depicted by Fig. 12b. The geometric constraints were not active in all the examples using this formulation. Employing the second formulation, the final configuration of inductors depends on the value of the parameter ψ_0. For the larger value, Fig. 13a shows the inductors obtained and Fig. 13b depicts the equilibrium shape and some level

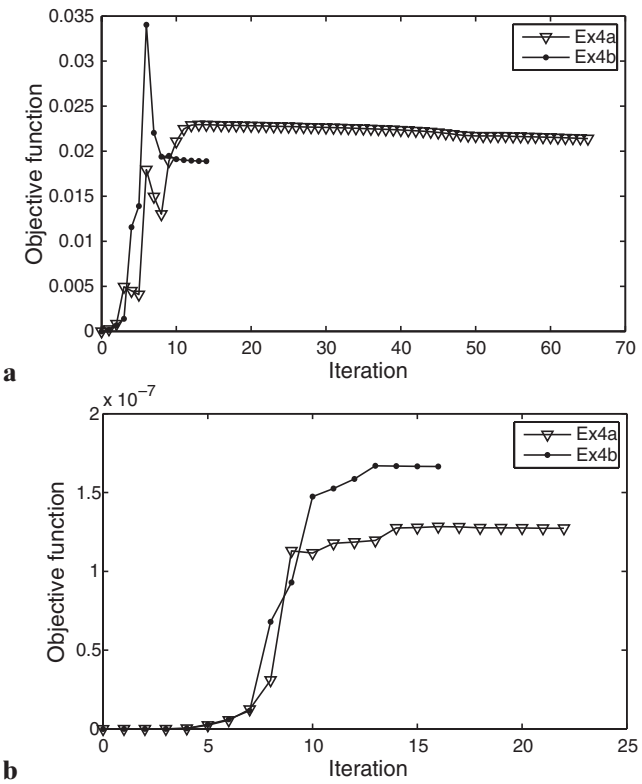

Fig. 23 Example 4, evolution of the objective functions, **a** first formulation, **b** second formulation

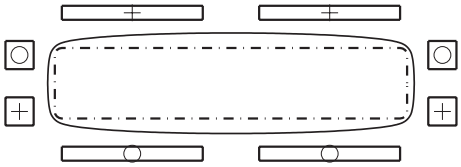

Fig. 24 Example 5, initial configuration. *Dash-dot line*: target shape, *solid line*: curves $\psi(x) = \psi_0$ for four different values of ψ_0, *plus*: inductor of positive current, *circle*: inductor of negative current

curves of the flux function φ at the solution. Figure 14 shows the same for the smaller value of ψ_0. Different from the first formulation, the second one has the solution having the inductors as close as the liquid metal as possible. In the four cases the geometric constraint is active. Although the location of the inductors is quite different using one or the other formulation, the optimum value of the objective function of the first formulation is almost the same for all the results obtained. The evolution of the objective function during the iterative process is shown by Fig. 15.

5.3 Example 3

The target shape of this example is the bar depicted by Fig. 16. For the inverse problem we consider eight inductors of type 1 of Fig. 3, and a target shape of area S_0 equal to 7.86. The intensity I is equal to 0.1 and the surface tension σ is equal to 1.0×10^{-4}. The dimensionless coefficients α_p have absolute value equal to 4.0 with the sign given by Fig. 16. The solutions for two different values of the parameter ψ_0, named Ex3a and Ex3b, are compared.

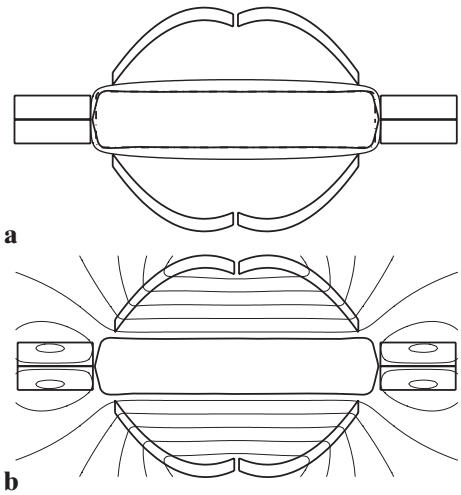

Fig. 25 Solution of the example Ex5, first formulation, **a** solution and geometric constraint, **b** equilibrium shape and level curves of the flux function φ

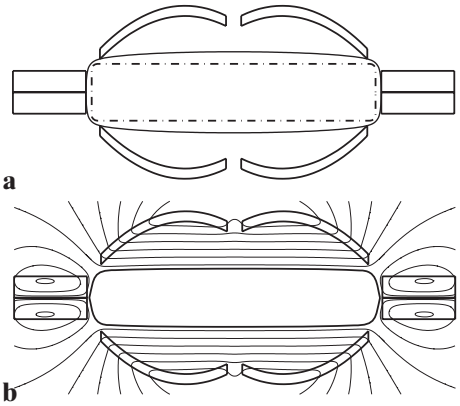

Fig. 26 Solution of the example Ex5, second formulation, **a** solution and geometric constraint, **b** equilibrium shape and level curves of the flux function φ

In this example, the main difference employing one or the other formulation is the size of the inductors located on the left and right sides. This size depends strongly on the value of the parameter ψ_0 when using the first formulation but weekly employing the second one. For the larger value and for the first formulation, Fig. 17a shows the inductors obtained and Fig. 17b depicts the equilibrium shape and some level curves of the flux function φ at the solution. Figure 18 shows the

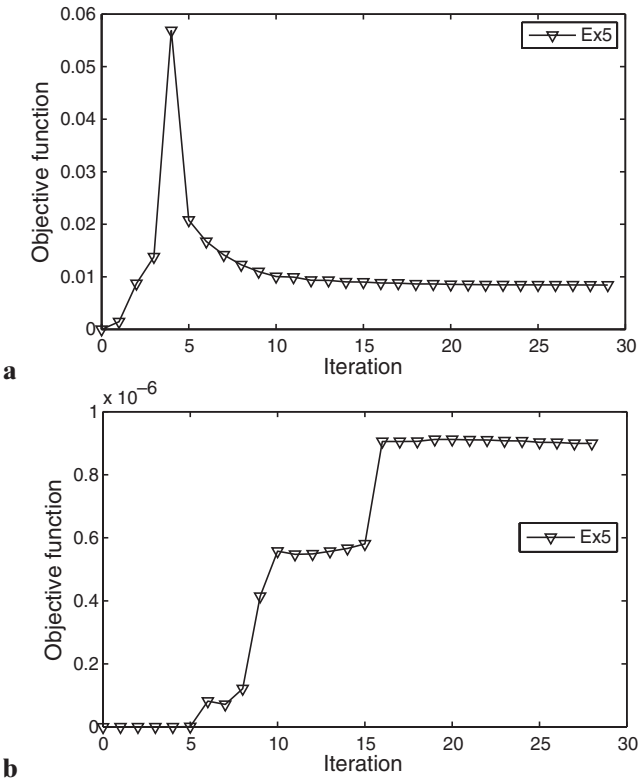

Fig. 27 Example 5, evolution of the objective functions, **a** first formulation, **b** second formulation

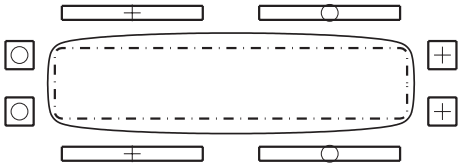

Fig. 28 Example 6, initial configuration. *Dash-dot line*: target shape, *solid line*: curves $\psi(x) = \psi_0$ for four different values of ψ_0, *plus*: inductor of positive current, *circle*: inductor of negative current

same for the second formulation. Figure 19 shows the evolution of the objective function during the iterative process.

5.4 Example 4

In this example the only difference with respect to the previous one is the sign of the coefficients α_p as depicted by Fig. 20. For the larger value of the parameter ψ_0 and for the first formulation, Fig. 21a shows the inductors obtained and Fig. 21b depicts the equilibrium shape and some level curves of the flux function φ at the solution. Figure 22 shows the same for the second formulation. The evolution of the objective function during the iterative process is shown by Fig. 23.

5.5 Example 5

The target shape of this example is the bar depicted by Fig. 24. For the inverse problem we consider eight inductors. The inductors on the top and bottom sides are of type 3 of Fig. 3 while the inductors on the left and right sides are of type 1. The target shape has S_0 equal to 4.99, the intensity I is equal to 0.1 and the surface tension σ is equal to 1.0×10^{-4}. The dimensionless coefficients α_p have absolute value equal to 4.0 with the sign given by Fig. 24.

Figure 25a shows the inductors obtained for the first formulation, and Fig. 25b depicts the equilibrium shape and some level curves of the flux function φ at the solution. Figure 26 shows the same for the second

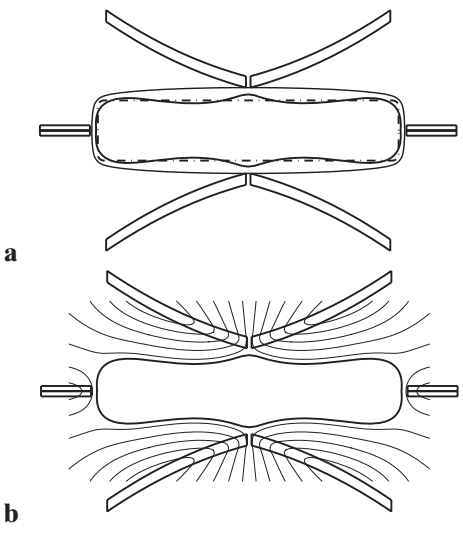

Fig. 29 Solution of the example Ex6, first formulation, **a** solution and geometric constraint, **b** equilibrium shape and level curves of the flux function φ

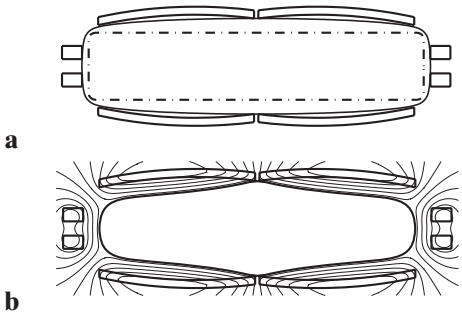

Fig. 30 Solution of the example Ex6, second formulation, **a** solution and geometric constraint, **b** equilibrium shape and level curves of the flux function φ

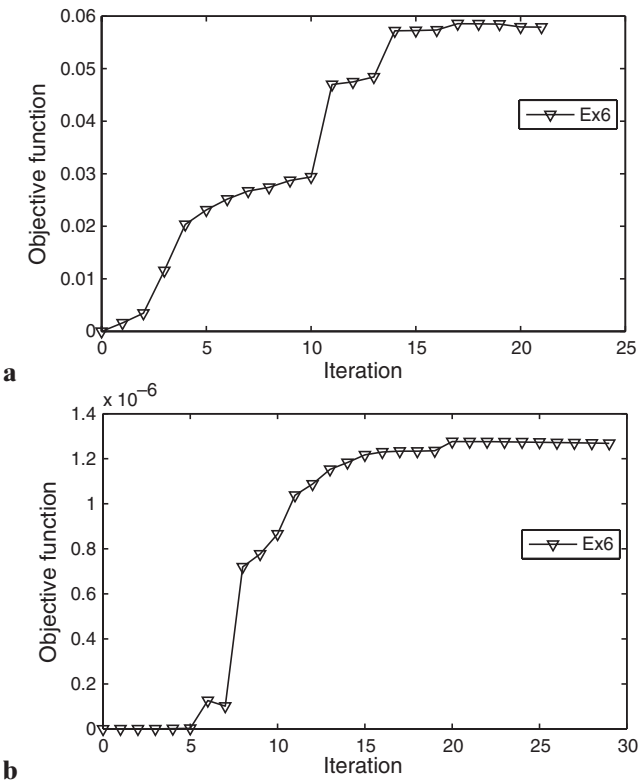

Fig. 31 Example 6, evolution of the objective functions, **a** first formulation, **b** second formulation

Table 1 Summary of results

Example	Nodes	Inductors	First formulation		Second formulation[a]		
			Iterations	Obj. F1[b]	Iterations	Obj. F1[b]	Obj. F2[b]
Ex1a	72	4	42	4.663e-07	48	1.773e-07	3.787e-11
Ex1b	72	4	58	7.267e-07	114	1.791e-07	3.777e-11
Ex2a	80	4	52	1.507e-04	93	1.640e-04	2.338e-08
Ex2b	80	4	52	1.507e-04	325	1.723e-04	3.535e-08
Ex2c	80	4	53	1.507e-04	318	1.964e-04	4.268e-08
Ex2d	80	4	53	1.507e-04	77	2.223e-04	4.731e-08
Ex3a	120	8	20	7.345e-04	20	1.135e-02	1.005e-07
Ex3b	120	8	21	4.513e-03	24	1.857e-02	1.142e-07
Ex4a	120	8	65	2.119e-02	22	9.728e-02	1.273e-07
Ex4b	120	8	14	7.712e-02	16	2.261e-01	1.663e-07
Ex5	136	8	29	8.558e-03	28	2.110e-02	8.988e-07
Ex6	136	8	21	5.513e-02	29	5.921e-01	1.260e-06

[a]Objective function of the first formulation calculated by a free-surface analysis considering the inductors obtained
[b]F1: first formulation, F2: second formulation

formulation. Figure 27 shows the evolution of the objective function during the iterative process.

5.6 Example 6

In this example the only difference with respect to the previous one is the sign of the coefficients α_p as depicted by Fig. 28. For the larger value of the parameter ψ_0 and for the first formulation, Fig. 29a shows the inductors obtained and Fig. 29b depicts the equilibrium shape and some level curves of the flux function φ at the solution. Figure 30 shows the same for the second formulation. As the figures show, the solutions of the considered formulations are very different in this case. This shows that the results of the second formulation have to be used with caution, they can be quite different from the best designs of the first formulation. The evolution of the objective function during the iterative process is shown by Fig. 31.

5.7 Summary of results

Table 1 resumes the information about the considered examples. For each one we give the number of nodes used for the finite element approximation of the boundary Γ^* of the target shape and the number of inductors. For each formulation the number of iterations performed by the optimization algorithm is indicated as well as the final value of the objective function. For the second formulation, the final value of the objective function of the first formulation is also indicated, it was calculated solving the free-surface problem considering the inductors obtained by the optimization algorithm. As one could expect, the first formulation shows smaller values of its objective function in all the examples with the only exception of the examples Ex1a and Ex1b where the shape of the inductors at the solution is almost the same.

6 Conclusions

This paper deals with the shape design of the inductors used in the electromagnetic casting of molten metals. Two different approaches based on nonlinear optimization have been proposed in order to find the position and shape of suitable inductors. The first one minimizes the difference between the geometries of the best possible equilibrium domain and the target shape; the second minimizes a slack variable function related to the equilibrium equation on the target boundary. We have also shown how to consider geometric constraints that prevent the inductors from penetrating the liquid metal. The finite dimensional optimization problems obtained after discretization were solved employing the line search interior-point algorithm FAIPA.

Some exhibited examples show that both formulations are effective to design suitable inductors. However, the formulations are not equivalent judging by the results obtained for the examples Ex2a-Ex2d and Ex6. In particular, the last example shows that the solution of the second formulation can be, qualitatively, quite different from the best design of the first one.

In terms of accuracy, the first formulation has performed better for almost all the examples. However, the final value of the objective function is only slightly different when using the second one. On the other hand, the second formulation has the advantage of being less time consuming, because of the lack of the shape variables related to the liquid metal. Thus, as most of the results are similar, this formulation appears to be interesting for finding an initial guess for the first formulation.

In contrast to the results obtained for the example Ex5, for the example Ex6 both formulations fail to find an accurate result. This fact shows the importance of the initial configuration of inductors. Therefore, it would be meaningful a solution method for finding

good initial configurations. As further study, we will consider this subject by means of topology optimization techniques.

Acknowledgements The authors would like to thank the Brazilian Research Councils CAPES, CNPq and Faperj for the financial support. The first author is supported by the grant E-26/100.280/2007 of Faperj. The second author would like to thank the French Research Councils COFECUB, INRIA and CNRS for the financial support.

References

Achtziger W (2007) On simultaneous optimization of truss geometry and topology. Struct Multidiscipl Optim 33(4–5): 285–304

Allaire G (2007) Conception optimale de structures, mathématiques and applications, vol 58. Springer, Berlin

Arora JS, Wang Q (2004) Optimization of large-scale structural systems using sparse SAND formulations. Tech. rep., Optimal Design Lab/CCAD, College of Engineering/4110 SC, The University of Iowa, Iowa City, IA 52242

Arora JS, Wang Q (2005) Review of formulations for structural and mechanical system optimization. Struct Multidiscipl Optim 30(4):251–272

Brancher JP, Séro-Guillaume OE (1985) Étude de la déformation d'un liquide magnétique. Arch Ration Mech Anal 90(1):57–85

Canelas A, Herskovits J, Telles JCF (2007) Shape optimization using the boundary element method and a SAND interior point algorithm for constrained optimization. Comput Struct 86(13–14):1517–1526

Canelas A, Roche JR, Herskovits J (2008) The inverse electromagnetic shaping problem. Struct Multidiscipl Optim. doi:10.1007/s00158-008-0285-9

Choi KK, Kim NH (2004) Structural sensitivity analysis and optimization 1 and 2. Springer, Berlin Heidelberg New York

Coulaud O, Henrot A (1994) Numerical approximation of a free boundary problem arising in electromagnetic shaping. SIAM J Numer Anal 31(4):1109–1127

Felici TP, Brancher JP (1991) The inverse shaping problem. Eur J Mech B Fluids 10(5):501–512

Fu HZ, Shen J, Liu L, Hao QT, Li SM, Li JS (2004) Electromagnetic shaping and solidification control of Ni-base superalloys under vacuum. J Mater Process Technol 148(1):25–29

Gagnoud A, Etay J, Garnier M (1986) Le problème de frontière libre en lévitation électromagnétique. J Méc Théor Appl 5(6):911–934

Haftka RT (1985) Simultaneous analysis and design. AIAA J 23(7):1099–1103

Haftka RT, Kamat MP (1989) Simultaneous nonlinear structural analysis and design. Comput Mech 4(6):409–416

Henrot A, Pierre M (1989) Un probléme inverse en formage de métaux liquides. Modél Math Anal Numér 23(1):155–177

Henrot A, Brancher JP, Pierre M (1989) Existence of equilibria in electromagnetic casting. In: Proceedings of the fifth international symposium on numerical methods in engineering. Comput Mech, vol 1, 2 (Lausanne, 1989). Southampton, pp 221–228

Herskovits J (1998) Feasible direction interior-point technique for nonlinear optimization. J Optim Theory Appl 99(1): 121–146

Herskovits J, Laporte E, Le Tallec P, Santos G (1996) A quasi-Newton interior point algorithm applied to constrained optimum design in computational fluid dynamics. Rev Européenne Élém Finis 5(5–6):595–617

Herskovits J, Mappa P, Goulart E, Mota Soares CM (2005) Mathematical programming models and algorithms for engineering design optimization. Comput Methods Appl Mech Eng 194(30–33):3244–3268

Kress R (1999) Linear integral equations, applied mathematical sciences, vol 82, 2nd edn. Springer, New York

Moffatt HK (1985) Magnetostatic equilibria and analogous Euler flows of arbitrarily complex topology I Fundamentals. J Fluid Mech 159:359–378

Murat S, Simon J (1976) Sur le contrôle par un domaine géométrique. Tech rep 76015, Laboratoire d'Analyse Numérique, Université de Paris

Nédélec JC (1977) Approximation des équations intégrales en mécanique et en physique. Tech rep, Centre de mathématiques appliquées, Ecole Polytechnique

Novruzi A (1997) Contribution en optimization de formes et applications. PhD thesis, Université Henri Poincaré, Nancy 1

Novruzi A, Pierre M (2002) Structure of shape derivatives. J Evol Equ 2(3):365–382

Novruzi A, Roche JR (1995) Second order derivatives, Newton method, application to shape optimization. Tech. Rep. RR-2555, INRIA

Novruzi A, Roche JR (2000) Newton's method in shape optimisation: a three-dimensional case. BIT 40(1):102–120

Pierre M, Roche JR (1991) Computation of free surfaces in the electromagnetic shaping of liquid metals by optimization algorithms. Eur J Mech B Fluids 10(5):489–500

Pierre M, Roche JR (1993) Numerical simulation of tridimensional electromagnetic shaping of liquid metals. Numer Math 65(2):203–217

Pierre M, Rouy E (1996) A tridimensional inverse shaping problem. Comm Partial Differ Equ 21(7–8):1279–1305

Roche JR (1996) Algorithmes numériques en optimization de formes et électromagnétisme, mémoire d'Habilitation à Diriger des Recherches

Roche JR (1997) Gradient of the discretized energy method and discretized continuous gradient in electromagnetic shaping simulation. Appl Math Comput Sci 7(3):545–565

Séro-Guillaume OE, Zouaoui D, Bernardin D, Brancher JP (1992) The shape of a magnetic liquid drop. J Fluid Mech 241:215–232

Shercliff JA (1981) Magnetic shaping of molten metal columns. Proc R Soc Lond A 375:455–473

Simon J (1980) Differentiation with respect to the domain in boundary value problems. Numer Funct Anal Optim 2(7–8): 649–687

Sneyd AD, Moffatt HK (1982) Fluid dynamical aspects of the levitation-melting process. J Fluid Mech 117:45–70

Sullivan CR (1999) Optimal choice for number of strands in a Litz-wire transformer winding. IEEE Trans Power Electron 14(2):283–291

Yi SI, Shin JK, Park GJ (2008) Comparison of MDO methods with mathematical examples. Struct Multidiscipl Optim 35(5):391–402

Zhiqiang C, Fei J, Xingguo Z, Hai H, Junze J (2002) Microstructures and mechanical characteristics of electromagnetic casting and direct-chill casting 2024 aluminum alloys. Mater Sci Eng A 327(2):133–137

Zouaoui D, Séro-Guillaume OE, Brancher JP (1990) Equilibrium of a magnetic liquid drop: variational approach and computation. Magn Gidrodin 26(4):32–35, 150